# XVI. Early Galaxy Formation and JWST Mass-Growth Tension

The formation and evolution of galaxies represent one of the most direct observational manifestations of cosmic structure growth and provide a critical testing ground for cosmological models. Within the standard ΛCDM framework, galaxies form hierarchically as small density perturbations in the primordial matter distribution grow through gravitational instability. Dark matter collapses first, forming virialized halos that act as gravitational potential wells into which baryonic matter falls. Gas accretion, radiative cooling, and angular momentum redistribution then enable the formation of rotationally supported disks and spheroidal stellar components. Over cosmic time, mergers, feedback processes, and secular evolution further shape galactic structure, leading to the diverse population of galaxies observed in the present-day Universe.

Observationally, galaxy evolution has been mapped across a wide range of redshifts through deep surveys conducted with ground-based telescopes and space observatories such as the Hubble Space Telescope. These studies have established robust trends in galaxy size, stellar mass, star formation rate, metallicity, and morphology as functions of redshift. At moderate redshifts ($z \lesssim 3$), galaxies are observed to grow steadily in stellar mass, with star formation rates that peak around $z \sim 2$ and decline toward the present epoch. Morphological transformations, including the emergence of bulge-dominated systems and quiescent ellipticals, are commonly associated with mergers, environmental effects, and feedback from supernovae and active galactic nuclei. Taken together, these observations have largely supported a picture of gradual, regulated galaxy growth embedded within an expanding Universe dominated by dark matter and dark energy.

From a theoretical perspective, the evolution of galaxy structure is governed by a complex interplay of physical processes operating across a wide range of spatial and temporal scales. Gas cooling and star formation occur on sub-kiloparsec scales, while halo growth and mergers unfold over cosmological volumes. Feedback mechanisms—such as stellar winds, supernova explosions, and radiation pressure—play a crucial role in regulating star formation efficiency and redistributing baryons within and beyond halos. As a result, galaxy evolution models rely on a combination of analytic prescriptions, numerical simulations, and semi-empirical scaling relations to connect fundamental cosmological parameters to observable galaxy properties. Despite these complexities, the ΛCDM paradigm has proven remarkably successful in reproducing the broad statistical properties of galaxies across most of cosmic history.

The advent of the James Webb Space Telescope has extended observational access to the earliest phases of galaxy formation, probing redshifts beyond $z \sim 10$ and into the first few hundred million years after the Big Bang. JWST observations have revealed candidate and spectroscopically confirmed galaxies at epochs previously thought to be dominated by small, chemically primitive systems. Some of these early galaxies appear unexpectedly luminous and massive given the limited cosmic time available for star formation and mass assembly. These findings highlight the importance of reassessing assumptions about star formation efficiency, gas accretion rates, feedback strength, and the initial conditions of galaxy formation in the early Universe.

Importantly, the detection of massive and luminous galaxies at very high redshift does not, by itself, imply a failure of the standard cosmological model. Rather, it underscores the need to carefully quantify the physical limits imposed by cosmic time, baryon availability, and feedback processes. At extreme redshifts, even modest changes in star formation efficiency or halo growth rates can lead to large differences in observable galaxy properties. Consequently, early galaxy observations provide a sensitive probe of the high-redshift regime where standard scaling relations may approach their limits of applicability.

In this context, simplified or "toy" models of early galaxy formation serve a valuable diagnostic role. By isolating key parameters—such as halo growth, baryon inflow, star formation efficiency, and outflow strength—such models allow one to explore the conditions under which early galaxies can assemble substantial stellar mass within a short time. These approaches do not seek to replace detailed numerical simulations, but rather to clarify the parameter space consistent with observations and to identify where tensions may arise. The implications of recent JWST discoveries for early galaxy growth, including quantitative mass–growth constraints inferred from high-redshift systems, are examined in detail in Section XXVIII.

## A. Structural Measurement Methods: Non Parametric

Recent measurement technique involves the non-parametric method of measuring galaxy light distributions. Non-parametric methods of measuring galaxy structure began in the photographic era with attempts to quantify the light concentration in galaxies by Morgan (1962), although extensive quantitative measures were not done until the mid-1990s. At present, the most common methods for measuring galaxy structure in a non-parametric way is through the CAS system (e.g., Conselice 2003) and through similar parameters (Takamiya 1999). These parameters are designed to capture the major features of the underlying structures of these galaxies, but in a way that does not involve assumptions about the underlying form, as is done with the S´ersic fitting.

**Asymmetry Index.** One of the more commonly used indices is the asymmetry index(A) which is a measure of how asymmetric a galaxy is after rotating along the line of sight center axis of the galaxy by 180 deg (Figure 2). It can be thought of as an indicator of what fraction of the light in a galaxy is in non-symmetric components. The basic formula for calculating the asymmetry index (A) is given by:

$$A = \min\left(\frac{\Sigma|I_0 - I_{180}|}{\Sigma|I_0|}\right) - \min\left(\frac{\Sigma|B_0 - B_{180}|}{\Sigma|I_0|}\right)$$

Where $I_0$ represents is the original galaxy image, $\boldsymbol{I_{180}}$ is the image after rotating it from its center by 180°. The measurement of the asymmetry parameter however involves several steps beyond this simple measure. This includes carefully dealing with the background noise in the same way that the galaxy itself is by using a blank background area ($B_0$), and finding the location for the center of rotation. The radius is usually defined as the Petrosian radius at which $\eta(R) = 0.2$, although once out to large radius the measured parameters are remarkably stable. Operationally, the area $B_0$ is a blank part of the sky near the galaxy. Typical asymmetry values for nearby galaxies are discussed in Conselice (2003) with ellipticals having values A ~ 0.02 ± 0.02, while spiral galaxies are found in the range from A ~ 0.07 − 0.2, while for Ultra-Luminous Infrared Galaxies (ULIRGs), which are often mergers, the average is A ~ 0.32 ± 0.19, and for merging starbursts A ~ 0.53 ± 0.22

**Galaxy Morphology and Structure** allows a new way to compare with cosmologically based galaxy formation models, as well as those which include extensive physics such as starformation, AGN feedback and supernova in more detailed hydrodynamical models.

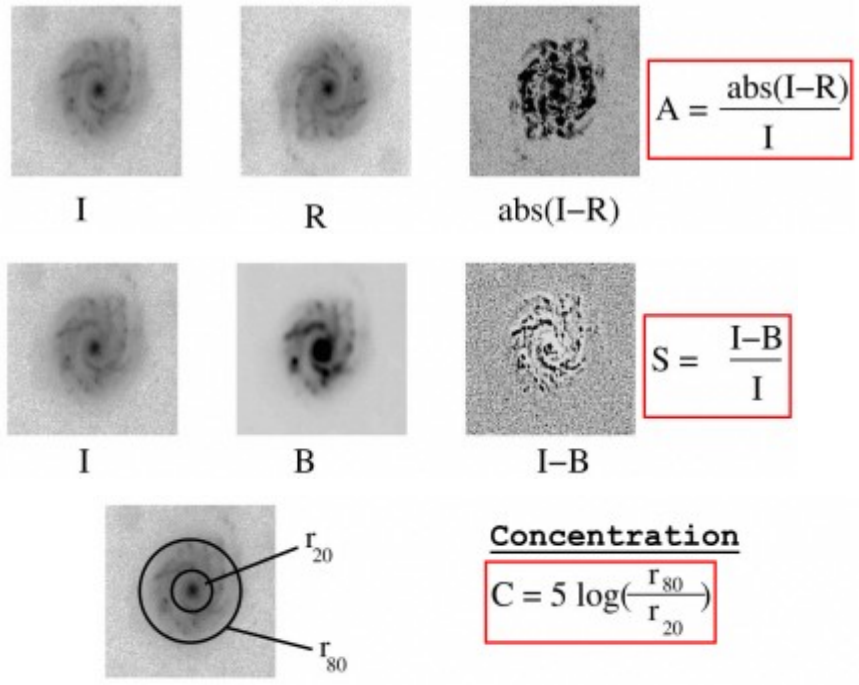


A graphical representation of how the concentration (C), asymmetry (A), clumpiness (S) are measured on an example nearby galaxy. Within the measurements for A and S, the value '***I***' represents the original galaxy image, while '***R***' is this image rotated by 180 deg. For the clumpiness S, 'B' is the image after it has been smoothed (blurred) by the factor $0.3 \times r(\eta = 0.2)$. The details of these measurements can be found in Conselice et al. (2000a) for asymmetry, A, Bershady et al. (2000) for concentration, C, and Conselice (2003) for the clumpiness index, S.

## B. Galaxy Type Classification

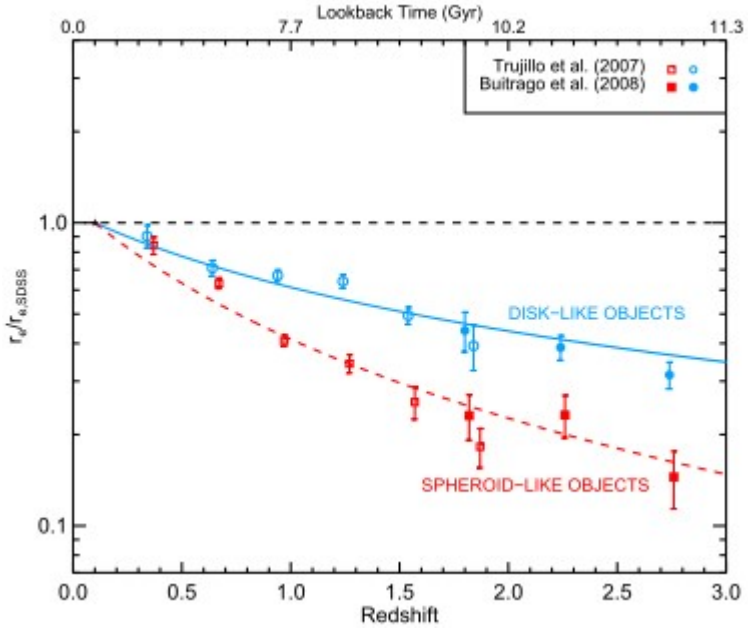


The average sizes of massive galaxies selected with Stellar Mass, $M* > 10^{11}$ $M_{\odot}$ as imaged in the POWIR (Conselice et al. 2007) $z < 2$ data and GNS > 1.5 images (Buitrago et al. 2008; Conselice et al. 2011). The size evolution is divided into galaxies with elliptical-like profiles, with Sersic indices (See below) $n > 2.5$, and disk-like profiles having $n < 2.5$. The measured effective radius, $r_e$ , is plotted as a function of the ratio with the average size of galaxies at the same stellar mass measurements with $M* > 10^{11}$ $M_{\odot}$ at $z = 0$ from Shen et al. (2003).

**The Sérsic Index** controls the degree of curvature of the profile. The smaller the value, the less centrally concentrated the profile is and the shallower (steeper) the logarithmic slope at small (large) radii.

The average concentration (C), asymmetry (A), and clumpiness (SS) parameters for nearby galaxies as measured in the optical R-band (Conselice 2003).

| Galaxy Type | Concentration (R) | Asymmetry (R) | clumpiness (R) |
|---|---|---|---|
| Ellipticals | 4.4±0.3 | 0.02±0.02 | 0.00±0.04 |
| Early-type disks (Sa-Sb) | 3.9±0.5 | 0.07±0.04 | 0.08±0.08 |
| Late-type disks (Sc-Sd) | 3.1±0.4 | 0.15±0.06 | 0.29±0.13 |
| Irregulars | 2.9±0.3 | 0.17±0.10 | 0.40±0.20 |
| Edge-on Disks | 3.7±0.6 | 0.17±0.11 | 0.45±0.20 |
| ULIRGs | 3.5±0.7 | 0.32±0.19 | 0.50±0.40 |
| Starbursts | 2.7±0.2 | 0.53±0.22 | 0.74±0.25 |
| Dwarf Ellipticals | 2.5±0.3 | 0.02±0.03 | 0.00±0.06 |

The clumpiness (or smoothness) (***S***) parameter is used to describe the fraction of light in a galaxy which is contained in clumpy distributions. Clumpy galaxies have a relatively large amount of light at high spatial frequencies, whereas smooth systems, such as elliptical galaxies contain light at low spatial frequencies. Galaxies which are undergoing star formation tend to have very clumpy structures, and thus high S values.

The original image $\boldsymbol{I_{x,y}}$ is blurred to produce a secondary image, $\boldsymbol{I^{\sigma}_{x,y}}$ The size of the smoothing kernel σ is determined by the radius of the galaxy,

$$S = 10 \times \left[ \left( \frac{\Sigma(I_{x,y} - I^{\sigma}_{x,y})}{\Sigma I_{x,y}} \right) - \left( \frac{\Sigma(B_{x,y} - B^{\sigma}_{x,y})}{\Sigma I_{x,y}} \right) \right]$$

# Early Galaxy Formation (Toy Model)

## Overview

**Computations Python Program:** **VXPhysics.com/Python/Early Galaxy Formation.py**

These figures illustrate a simplified ("toy") model of early galaxy formation in a ΛCDM cosmology, tracking the **coupled evolution of dark matter halos, baryonic gas, star formation, and chemical enrichment** from redshift $z \approx 25$ to $z \approx 6$.

### Halo growth

Evolution of the dark matter halo mass as a function of redshift. The rapid growth at high redshift reflects the hierarchical nature of structure formation, where halos accrete mass efficiently due to the high cosmic density and merger rate in the early universe.

$$\dot{M}_{\rm halo} \approx K \left( \frac{M}{10^{12} M_\odot} \right)^{1.1} (1+z)^{2.5} \, M_\odot/\mathrm{yr}$$

Key physical idea:

Dark matter collapses first and provides the gravitational potential well that enables baryonic galaxy formation.

### Baryon reservoirs

Evolution of the stellar mass (solid line) and cold gas mass (dotted line) within the halo. Gas is accreted from the halo, converted into stars through star formation, and depleted by stellar feedback-driven outflows.

Key physical idea:

Galaxy growth is governed by a competition between gas inflow, star formation, and feedback.

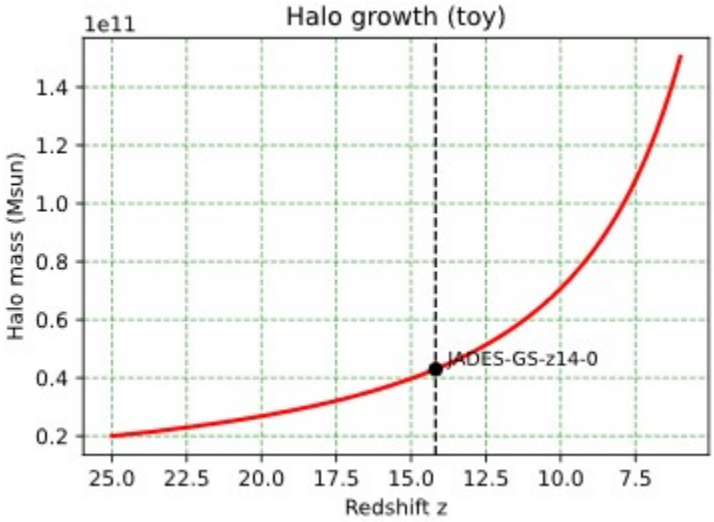


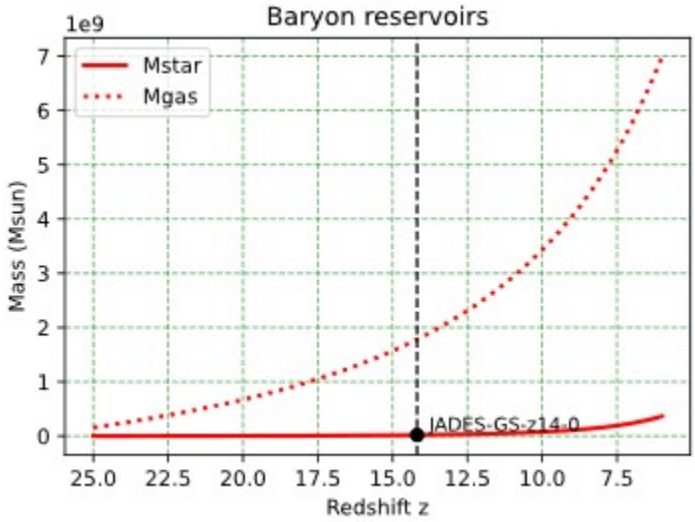


## JWST Mass-Growth Tension: Galaxy Growth Dynamics

### Dark matter halo formation (foundation)

**What it represents**

- The gravitational scaffolding where galaxies form
- Collapse of overdensities after recombination

**Gas infall & cooling (first baryons)**

**What it represents**

- Gas falling into dark matter halos
- Cooling via atomic hydrogen, molecular hydrogen ($H_2$)

**What you can program**

- Cooling time vs halo mass
- Virial temperature thresholds
- Gas accretion rates

$$t_{\rm cool} \sim \frac{3kT}{n\Lambda(T)}$$

**Black hole seeds & early growth**

**Classic growth law:** $M(t) = M_0 e^{t/t_E}$

**How gas turns into stars when density exceeds a threshold**

- Schmidt-Kennicutt laws
- Star-formation efficiency vs redshift
- Bursty vs steady star formation

**Simple model** $\dot{M}_\star = \epsilon \frac{M_{\rm gas}}{t_{\rm dyn}}$

**Chemical enrichment (metals appear fast)**

**Gas Metallicity: What it represents**

- Supernovae enriching gas with metals
- Transition from Pop III →Pop II stars
- Metallicity evolution
- Yield models
- Mixing timescales

$$Z(t) = \frac{M_Z(t)}{M_{\rm gas}(t)}$$

**Dynamics with the Following Graphs**

**Star formation rate**

Star formation rate (SFR) as a function of redshift, computed using a Schmidt-type star formation nal to the available cold gas mass. The elevated SFR at high redshift reflects the high gas densities and short dynamical times characteristic of early galaxies.

**See Above: Cooling time Classic growth law Gas Metallicity**

Key physical idea:

Early galaxies can form stars very rapidly, producing intense, bursty star formation episodes.

**Gas metallicity (toy)**

Evolution of the gas-phase metallicity, showing the progressive chemical enrichment of the interstellar medium by stellar nucleosynthesis. Metals are produced by short-lived massive stars and redistributed through feedback and gas flows.

Key physical idea:

Even very early galaxies can become chemically enriched on timescales of tens of Myr, consistent with metal detections in high-redshift JWST galaxies.

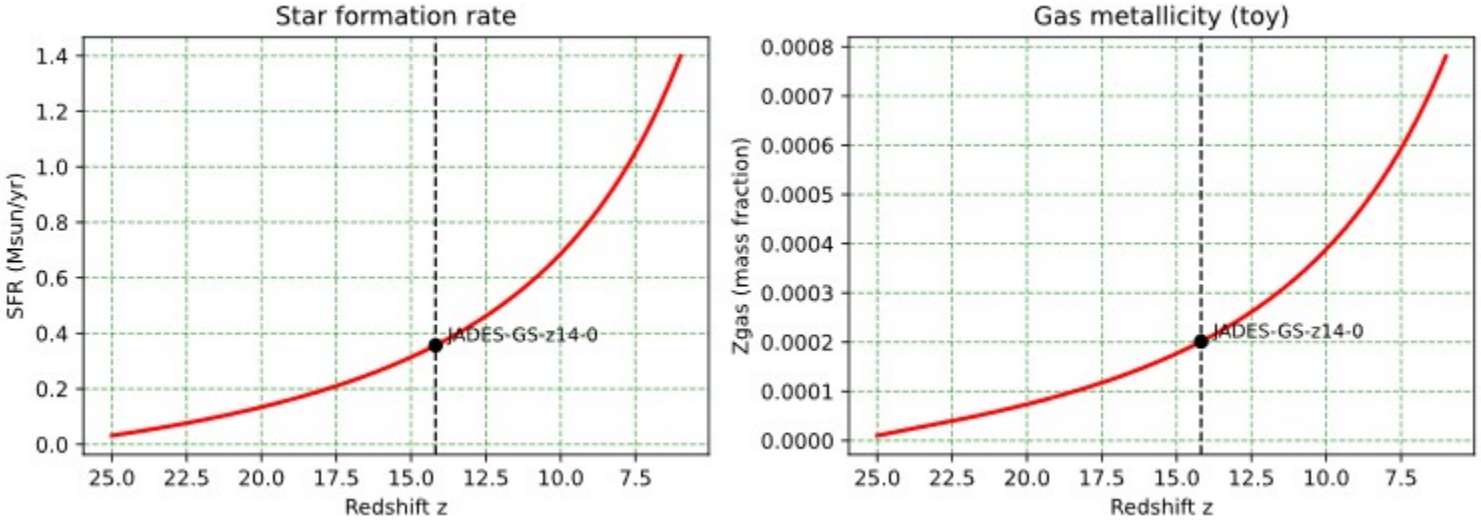


**Computations Python Program: VXPhysics.com/Python/JWST Mass–Growth Tension.py**

## JWST Mass-Growth Tension Diagnostics

Diagnostic plots illustrating the "mass-growth tension" implied by very massive, UV-luminous galaxies at z ≈ 10–15. The panels quantify (i) the average star-formation rate required to assemble a given stellar mass within the available cosmic time, (ii) a toy upper envelope for star formation set by baryonic supply and a star-formation efficiency prescription, (iii) the exponential growth of black-hole seeds under Eddington or super-Eddington accretion, and (iv) the age of the Universe as a function of redshift in a flat ΛCDM cosmology. Together these show how inferred stellar or black-hole masses at high redshift translate into stringent constraints on formation redshift, duty cycle, accretion efficiency, and feedback-regulated baryon conversion.

**Build $M_*$ by $z_{obs}$ — Required average SFR vs $z_{form}$**

*Required time-averaged star-formation rate $\langle \mathrm{SFR} \rangle$ needed to assemble a target stellar mass $M_*$ by an observed redshift $z_{obs}$, as a function of the assumed onset of star formation $z_{form}$. The curve steepens rapidly for later $z_{form}$ because the available cosmic time $\Delta t = t(z_{obs}) - t(z_{form})$ shrinks to tens of Myr at $z \gtrsim 10$. This panel highlights the basic "clock constraint": at fixed $M_*$, the inferred $\langle \mathrm{SFR} \rangle \propto 1/\Delta t$, so even modest increases in $M_*$ or delays in $z_{form}$ can require extreme SFRs or near-continuous duty cycles.*

### Toy SFR envelope at $z_{\rm obs}$ — Supply/efficiency limit

*Toy upper envelope for the star-formation rate at $z_{\rm obs}$ as a function of halo mass, based on a simple baryon supply assumption $M_{\rm gas} \sim f_{\rm in} f_b M_{\rm halo}$ and a Schmidt-type scaling $\mathrm{SFR} \sim \epsilon\, M_{\rm gas}/t_{\rm dyn}$. The dashed horizontal line marks the required $\langle \mathrm{SFR} \rangle$ from panel (a) for a representative $z_{\rm form}$. Intersections (or lack thereof) illustrate whether the implied stellar buildup is plausible for a given halo mass without invoking unusually high baryon inflow, star-formation efficiency, or suppressed feedback. This panel reframes the tension as a comparison between required growth and available baryonic throughput.*

## JWST Mass-Growth Tension Diagnostics

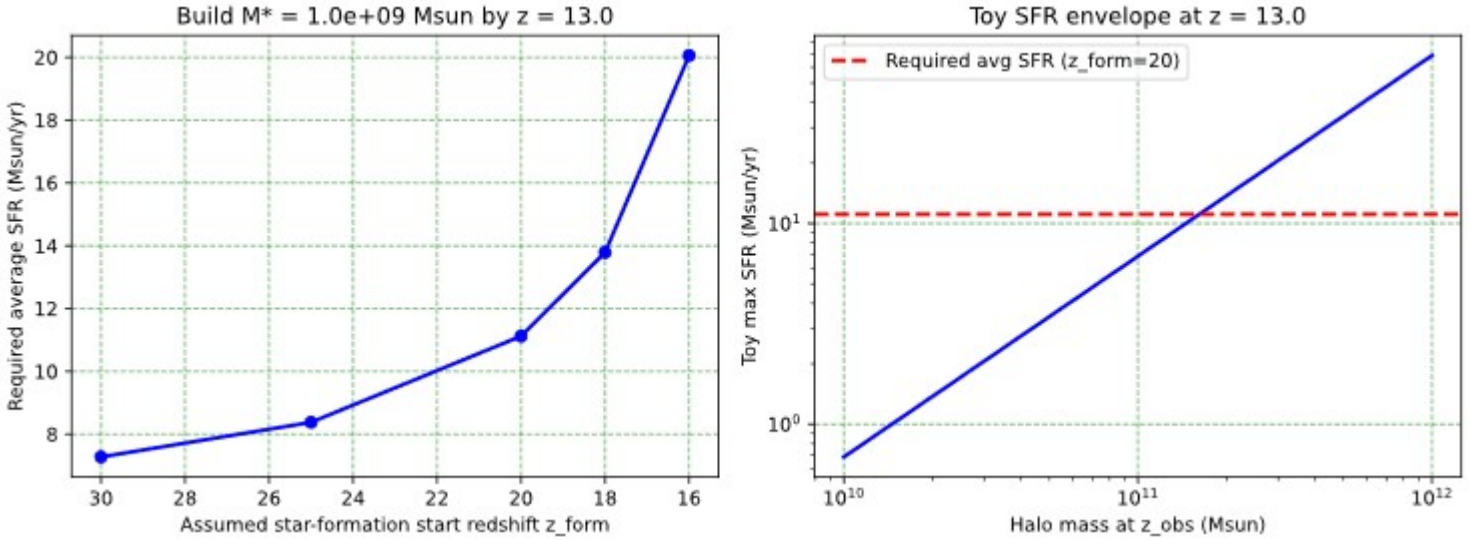


### BH growth from $z_{\rm start}$ to $z_{\rm end}$ — Eddington constraint

*Final black-hole mass achieved by seeds of different initial mass $M_0$ under sustained accretion at a fraction $f_{\rm Edd}$ of the Eddington rate, assuming radiative efficiency $\epsilon$. Growth is exponential, $M(t) = M_0 \exp(\Delta t/t_{\rm Salp})$, where $t_{\rm Salp}$ is the Salpeter timescale. The strong sensitivity to $f_{\rm Edd}$ and $M_0$ illustrates why early supermassive black holes can be challenging: reaching $10^{8-9} M_\odot$ at high redshift may require heavy seeds (e.g., direct-collapse scenarios), super-Eddington phases, low radiative efficiency, or high duty cycle.*

### Cosmic time vs redshift (flat ΛCDM) — the time budget

*Age of the Universe as a function of redshift in a flat ΛCDM cosmology, emphasizing that JADES-GS-z14-0 is observed only $\sim 280-300$ Myr after the Big Bang. The extremely short time intervals between $z \sim 20$ and $z \sim 14$ underpin the mass-growth tension: galaxies at these redshifts must form stars, enrich their gas, and build structure on timescales comparable to a single galactic dynamical time.*

## The Eddington constraint

states that there is a maximum luminosity—and therefore a maximum steady accretion rate—at which the outward force of radiation pressure on ionized gas exactly balances the inward force of gravity, limiting how rapidly mass can be accreted.

2. Physical balance behind the constraint

The Eddington limit arises from the balance between gravitational attraction acting on protons and radiation pressure acting primarily on electrons through Thomson scattering. When radiation pressure equals gravity, additional infalling material is prevented from accreting.

3. The Eddington luminosity

The Eddington luminosity is given by $L_{\rm Edd} = \frac{4\pi G M m_p c}{\sigma_T},$

which numerically evaluates to $L_{\rm Edd} \approx 1.26\times10^{38}\ (M/M_\odot)\ {\rm ergs}^{-1}$.

This represents the maximum steady luminosity for spherical accretion of ionized hydrogen.

4. Accretion rate associated with the Eddington limit

Relating luminosity to mass accretion via the Eddington accretion rate

where $\epsilon$ is the radiative efficiency, typically of order 0.1 for standard accretion disks.

$$L = \epsilon \dot{M} c^2,$$

5. The Eddington (Salpeter) timescale

If accretion proceeds continuously at the Eddington rate, mass grows exponentially with time. The characteristic e-folding timescale is known as the Salpeter time.

$$t_{\rm Salp} \approx 45\ {\rm Myr} \left(\frac{\epsilon}{0.1}\right).$$

6. Relevance to JWST-era galaxies

JWST observations reveal massive galaxies and black holes at redshifts $z \gtrsim 10$, when the Universe was only a few hundred million years old. The limited number of Eddington e-folding times available places strong constraints on how rapidly stars and black holes could have assembled.

7. Ways the constraint can be relaxed

The Eddington constraint is not absolute and may be alleviated through mechanisms such as super-Eddington accretion, reduced radiative efficiency, anisotropic radiation, high accretion duty cycles, or the presence of massive initial black-hole seeds formed by direct collapse.

8. Why it is a constraint rather than a strict law

The Eddington limit relies on simplifying assumptions, including spherical symmetry, steady accretion, and electron scattering opacity. Real astrophysical systems can temporarily exceed this limit, making it a useful benchmark rather than a strict physical prohibition.

**Summary**

The Eddington constraint provides a fundamental timescale and upper limit on mass growth by accretion, playing a central role in interpreting the rapid assembly of massive galaxies and black holes observed by JWST in the early Universe.

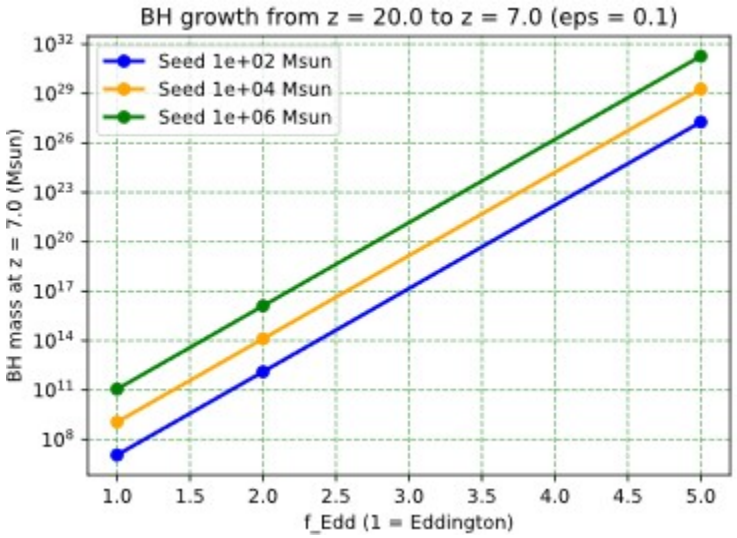


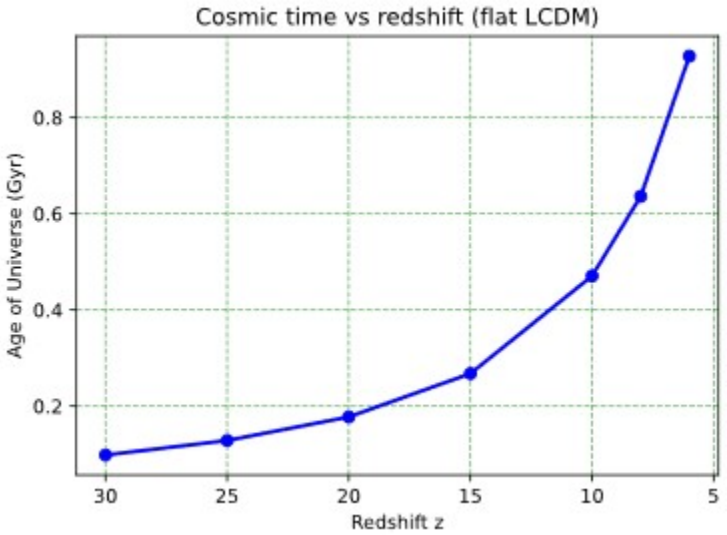

**z14: Spectroscopically confirmed at z ≈ 14. Very luminous and extended for such an early time.**

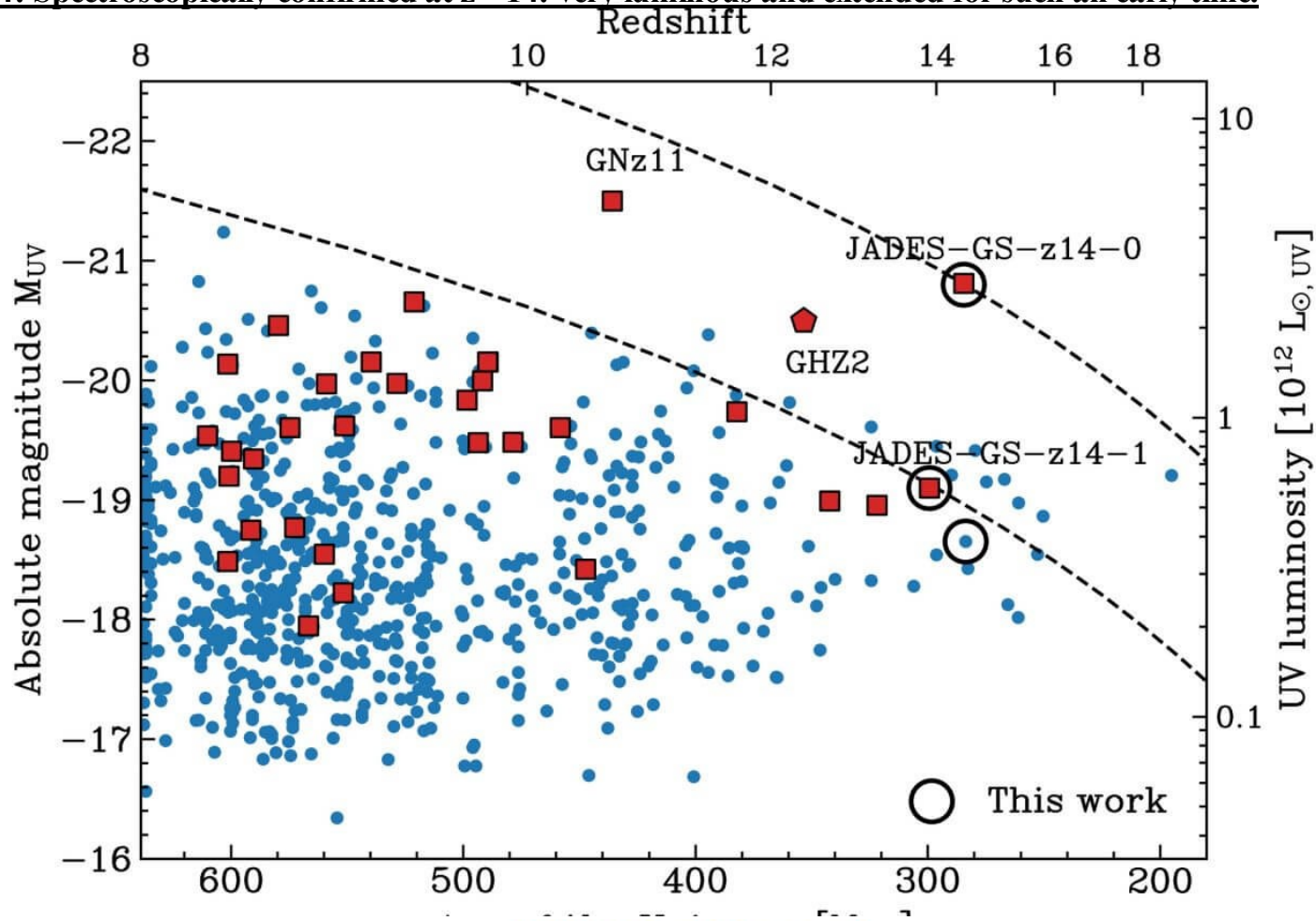


**JADES-GS-z14-0**